atmosphere

MDPI

Article

Intercomparison of Ambient Nitrous Acid Measurements in a Shanghai Urban Site

Zhenni Yang [1], Meng Wang [1], Yanping Hou [1,†], Yucun Liu [1,2,‡], Satheesh Chandran [3,§], Ravi Varma [3], Shengrong Lou [1,2] and Jun Chen [1,*]

[1] Shanghai Key Laboratory of Multiphase Flow and Heat Transfer in Power Engineering, School of Energy and Power Engineering, University of Shanghai for Science and Technology, Shanghai 200093, China; 192450035@st.usst.edu.cn (Z.Y.); 191450004@st.usst.edu.cn (M.W.); 132380041@st.usst.edu.cn (Y.H.); liuyucun@thunderchina.com (Y.L.); lousr@saes.sh.cn (S.L.)

[2] State Environmental Protection Key Laboratory of the Cause and Prevention of Urban Air Pollution Complex, Shanghai Academy of Environmental Science, Shanghai 200070, China

[3] Optind Solutions Private Limited, Unit No. 11, Technology Business Incubator, National Institute of Technology Calicut, Calicut 673601, India; satheesh.chandran@ucc.ie (S.C.); r.varma@nitc.ac.in (R.V.)

* Correspondence: j.chen@usst.edu.cn

† Current address: The Boiler & Pressure Vessel Safety Inspection Institute of Henan Province, Zhengzhou 450016, China.

‡ Current address: Shanghai Thunder Environmental Technology Co., Ltd., Shanghai 201404, China.

§ Current address: Physics Department and Environmental Research Institute, University College Cork, T12 YN60 Cork, Ireland.

Abstract: Nitrous acid (HONO) is the major source of OH radicals in polluted regions and plays a key role in the nitrogen cycle of the atmosphere. Therefore, accurate measurements of HONO in the atmosphere is important. Long Path Absorption Photometer (LOPAP) is a common and highly sensitive method used for ambient HONO measurements. Incoherent Broadband Cavity Enhanced Absorption Spectroscopy (IBBCEAS) is a recent alternative for the detection of HONO with high temporal and spatial resolutions, which has shown a detection limit of 0.76 ppbv at a sampling average of 180 s. In this study, LOPAP and IBBCEAS-HONO instruments were deployed in a Shanghai Urban Site (Shanghai Academy of Environmental Sciences) and simultaneously recorded the data from both instruments for a quantitative intercomparison of the measured atmospheric HONO for four days from 30 December 2017–2 January 2018. The HONO concentration measured by IBBCEAS and LOPAP were well matched. The campaign average concentrations measured by IBBCEAS and LOPAP were 1.28 and 1.20 ppbv, respectively. The intercomparison results demonstrated that both the IBBCEAS-HONO instrument and LOPAP-HONO instrument are suitable for ambient monitoring of HONO in a polluted urban environment.

Keywords: nitrous acid; IBBCEAS; LOPAP

check for updates

Citation: Yang, Z.; Wang, M.; Hou, Y.; Liu, Y.; Chandran, S.; Varma, R.; Lou, S.; Chen, J. Intercomparison of Ambient Nitrous Acid Measurements in a Shanghai Urban Site. *Atmosphere* **2022**, *13*, 329. https://doi.org/10.3390/atmos13020329

Academic Editors: Haichao Wang and Zhaofeng Tan

Received: 31 December 2021
Accepted: 12 February 2022
Published: 16 February 2022

Publisher's Note: MDPI stays neutral with regard to jurisdictional claims in published maps and institutional affiliations.

Copyright: © 2022 by the authors. Licensee MDPI, Basel, Switzerland. This article is an open access article distributed under the terms and conditions of the Creative Commons Attribution (CC BY) license (https://creativecommons.org/licenses/by/4.0/).

1. Introduction

Atmospheric nitrous acid (HONO) is an important nitrogen oxidation compound that produces hydroxyl radicals (OH) by photolysis in the near-UV wavelength band:

$$HONO + hv(300 - 400\text{nm}) \rightarrow NO + OH \quad (1)$$

HONO is considered as a major OH initiation source in polluted regions during the daytime [1,2] and is particularly important at sunrise [3,4]. Recent studies have shown that HONO contributes ~80% of the OH radicals during early morning hours and about 20–60% of the total regular OH [3–8]. HONO has an important influence on the oxidation capacity of the atmosphere, leading to the formation of secondary pollutants and accelerating the formation of air pollutants [9,10]. Since the first measurements of atmospheric HONO

were made by Nash in 1974 and Perner et al. in 1979 [11,12], HONO chemistry has proved essential to understanding the cycle of reactive nitrogen compounds in the troposphere [13].

Primary HONO sources include vehicular emissions [14], coal combustion emissions [15], and soil emissions [16]. The major secondary HONO sources are homogeneous reactions of OH with NO [17], heterogeneous reactions of NO_2 on the surface of particles and on the ground surface [18–20], the photolysis of HNO_3 and NO_3^- [21], and photolysis of nitro-phenols [22]. It is generally agreed that the heterogeneous NO_2 chemistry is probably among the most important sources of HONO [10,23,24]. In short, the measurement of gaseous HONO concentrations in the atmosphere and the analysis of its sources and sinks are of great atmospheric importance.

There are many methods available for detecting gaseous HONO in the atmosphere, including various physical and chemical methods such as Long Path Differential Optical Absorption Spectroscopy (LP-DOAS) [25], Cavity Ring-down Spectroscopy (CRDS) [26], Tunable Diode Laser Absorption Spectroscopy (TDLAS) [27], Incoherent Broadband Cavity Enhanced Absorption Spectroscopy (IBBCEAS) [28,29], Annular Denuder-IC [30], Mist Chamber-IC [25], and Long Path Absorption Photometer (LOPAP) [31,32]. Currently, IBBCEAS, LP-DOAS and LOPAP are widely used for ambient HONO measurements. The LP-DOAS allows for artifact-free (without air sampling) identification and quantification of HONO through its narrow band UV absorptions in the open atmosphere with detection limits in the range of 50–200 pptv [31,33]. However, this technique provides only averaged HONO concentration along the optical light path and thus has a low spatial resolution [12]. The LOPAP allows for online measurements of absolute HONO concentration with high sensitivity and a detection limit of ~0.2 pptv [34]. However, LOPAP might suffer from various limitations due to potential chemical interferences and longtime response for some specific applications [35]. The IBBCEAS offers the capacity of performing with sensitivity adequate for ambient sampling, is chemical interference-free, and has direct concentration measurements at high spatial resolution by local sampling without any sample preparation. This method uses a broadband incoherent light source (similar to a light emitting diode (LED) or xenon arc lamp) for broadband multispecies measurements. There exist some comparisons between IBBCEAS and other methods in a real atmospheric environment as follows: Wu et al. recorded the daytime and nighttime concentrations of HONO and NO_2 using LED-IBBCEAS and compared them with data from a LOPAP and a NO_x analyzer equipped with a blue light converter, in 2014. Intercomparisons of stripping coil–ion chromatograph (SC-IC) with other methods (CEAS and two LOPAPs) were conducted in field campaigns by Xue et al. in 2019 [36]. IBBCEAS was compared to that of extractive wet techniques, Long Path Absorption Photometry (LOPAP) and chemiluminescence (CL) NO_X detection by Dixneuf et al. in 2021 [37]. In addition, intercomparison measurements of HONO, NO_2 and CH_2O measured by IBBCEAS, NitroMAC and FTIR during the reaction of NO_2 with water vapor was performed in a CESAM chamber by Yi et al. in 2021 [38].

Two in-house built instrumentations, IBBCEAS and LOPAP, were adopted to carry out a series of performance characterizations and experiments in the laboratory where the response of the two instruments to HONO under the same experimental conditions were verified and compared. The two instruments were also included in the same period of atmospheric HONO concentration observations at the Shanghai Academy of Environmental Sciences (SAES), and the absolute values and trends of HONO concentrations measured by the two devices were analyzed and compared.

2. Principle and Experimental Setup

The IBBCEAS and LOPAP setup used in this work were developed in house. To ensure the reliability of the instruments, a series of performance characterizations: detection limits, residence times, calibrations, and stability, were carried out before field deployment in the laboratory of SAES.

2.1. LOPAP-HONO Setup and Performance Characterization

2.1.1. LOPAP-HONO Setup

Long Path Absorption Photometer (LOPAP) is a detection technology based on a solvent-modified Griess colorimetric method and spectrophotometry [31,39,40], which combines a chemical method with optical measurements to quantitatively measure HONO concentration.

During the past two decades, the LOPAP technique and equipment were generated and established by Heland et al., 2001 [31]; Kleffmann et al., 2006 [40]; Häseler et al., 2009 [41]; Chen et al., 2014 [32]; and Liu et al., 2016 [42]. Based on these new advances in LOPAP techniques adopted in this study, we established our LOPAP setup. Several schematic improvements were made to enhance the equipment performance as well as the operational and maintenance convenience. A schematic explaining the principle of the setup is shown in Figure 1a.

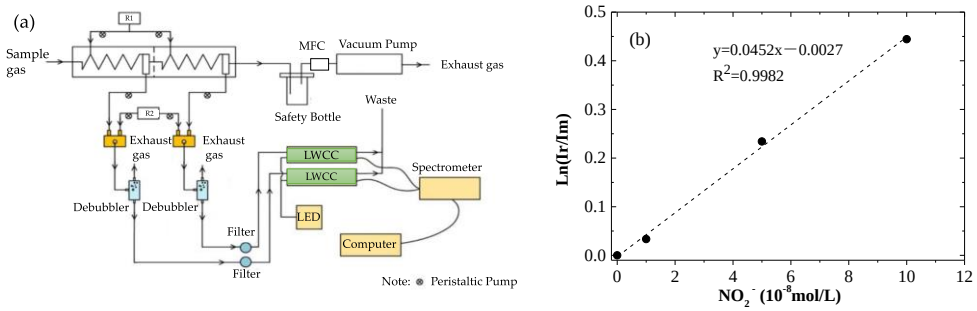


Figure 1. (**a**) Schematic of the LOPAP instrument. (**b**) Calibration curve of the LOPAP, where m represents the measured value and r represents the reference value.

The home-made LOPAP system consists of three separate units: (1) the external sampling unit, which is controlled by a Mass Flow Controller (MFC: Model CS200 Sevenstar Flow Co., Ltd.) and the diaphragm flow pump (KNF Neuberger, Inc. Freiburg, Germany) to ensure the inlet flow rate of sampler is precisely 1 L/min; (2) the wet chemical reaction unit in which the azodye is generated; (3) a dual-channel spectral detection unit that measures the concentration of azodye using a Long Path Absorption Method, thereby measure the HONO concentration.

There are two basic chemical reactions in the wet chemical reaction unit, HONO absorption and azodye formation. The sample gas was drawn through a double-channel stripping coil sampler. At the same time, absorption solution (R1) consisting of 0.06 mol/L sulfanilamide and 1 mol/L hydrochloric acid solution was pumped into the stripping coil sampler. The injection speeds of R1 solution are controlled at approximately 0.5 mL/min by a multi-channel peristaltic pump (T100-BM-24/DG-8-B). Meanwhile, the microflow meter records the precise actual flow rates in real time. The R1 solution will extract the HONO out of the sample gas and turn it into diazonium salt through reactions (2) and (3). Then, the diazonium salt solution and 0.8 mmol/L N-(1-Naphthyl) ethylenediamine dihydrochloride staining solution (R2) will be pumped into two three-way mixers, and the azodye formation takes place following Reaction (4) [43].

$$HONO + H^+ \leftrightarrow NO^+ + H_2O \quad (2)$$

$$NH_2\text{-}SO_2\text{-}C_6H_4\text{-}NH_2 + NO^+ \rightarrow NH_2\text{-}SO_2\text{-}C_6H_4\text{-}N_2^+ + H_2O \quad (3)$$

$$NH_2\text{-}SO_2\text{-}C_6H_4\text{-}N_2^+ + C_{10}H_7\text{-}NH\text{-}C_2H_4\text{-}NH_2[ClH]_2 \rightarrow NH_2\text{-}SO_2\text{-}C_6H_4\text{-}N=N\text{-}C_{10}H_6\text{-}NH_2\text{-}C_2H_4\text{-}NH_2[ClH]_2 \quad (4)$$

The dual-channel spectral detection unit consists of two sets of Liquid Waveguide Capillary Cells (LWCC) (World Precision Instrument, Sarasota, FL, USA) with optical path lengths of 100 and 250 cm to ensure the most sensitive detection limit of the setup,

with a transmission efficiency of 29.3% and 24.8% at 540 nm, respectively, spectrometers (STS-VIS, Ocean Optics, Dunedin, FL, USA), an adjustable fiber-coupled LED light, and two commercial debubblers. The tiny positive pressure in the pipeline of the spectral detection unit caused by the specially designed upstream-located peristaltic pump and the commercial debubbler can successfully eradicate the bubble in the pipeline without allowing liquid to escape, increasing the equipment's performance as well as the ease of operation and maintenance.

2.1.2. Calibration of LOPAP-HONO

The liquid phase calibration of the device is mainly used to establish the linear relationship between absorbance and liquid nitrite. Nitrite concentration is the key variable for calculating gas phase HONO concentration. The relationship between and absorbance is established by introducing nitrite solutions in different concentrations of R1 as dilution, which are pumped by the reagent feed line into the instrument.

The specific operations are as follows: (1) dilute 10^{-3} mol/L standard solution with ultrapure water to 10^{-4} mol/L, dilute with ultrapure water at constant volume, and the volumetric flask is 100 mL; (2) dilute 10^{-4} mol/L standard solution into10^{-6} mol/L mother liquor with absorption solution, dilute the absorption solution at constant volume, and the volumetric flask is 100 mL; (3) 10^{-6} mol/L mother liquor is proportioned into nitrite solutions of different concentrations according to the demand. The configuration process is constant volume dilution of the absorption solution, and the volumetric flask is 100 mL. The nitrite concentrations proportioned during the calibration process of the device are 0 mol/L, 10^{-8} mol/L, 5×10^{-8} mol/L, 10×10^{-8} mol/L; (4) switch the sampling gas of the unit to the N_2 and replace the absorption solution (R1) with the configured standard solution. After the standard solution entering the system reacts with the reaction solution, the linear relationship between absorbance and liquid nitrite is obtained. Since the response time of the device is 4 min, the time of each group of experiments is generally 15 to 20 min duration. If there is signal fluctuation in the calibration process, the calibration time should be extended. Figure 1b shows the calibration curves of LOPAP liquid phase calibration. The R^2 of the calibration plot is 0.9982, indicating that the instrument is currently in good condition. The reasons affecting the calibration curve include the configuration of absorption solution and reaction solution, the configuration of standard solution, the cleaning of instrument pipeline and LWCC, etc. [44].

2.2. IBBCEAS-HONO Setup and Performance Characterization

2.2.1. IBBCEAS-HONO Setup

IBBCEAS for HONO measurements was first developed by a research team from the University of Cork in Ireland in 2008 [28]. A series of IBBCEAS devices and studies for HONO measurements was also carried out later worldwide (Wu et al., 2014, Donaldson et al., 2014, Scharko et al., 2014, Min et al., 2016, Nakashima et al., 2017, Duan et al., 2018) [45–50].

The schematic representation of IBBCEAS-HONO instrument used in this study is shown in Figure 2a. The light from a stable LED (HSE365H-M807 HaSun Optoelectronics (HK) Co., Ltd., Hong Kong) was coupled to the optical cavity of the length L = 72.5 cm with the help of a lens (GCL-010811 Thorlabs). The optical cavity comprises two high-reflection mirrors (LayTec GmbH, Berlin, Germany) with reflectivity, R. ~0.9995 in 360–395 nm wavelength range. N_2 gas (99.99%, Dart (Shanghai) Gases Co., Ltd., Shanghai, China) is used as a purge to protect the cavity mirrors and as a zero gas controlled by the solenoid valve switch into the sampling pipeline. The light exiting the cavity was collected by a similar second lens and was coupled into a dispersive spectrometer (Ocean Insight QE series, Orlando, FL, USA) with the help of a multimode optical fiber (200 µm ∗ 7Cores; Ocean Optics, Dunedin, FL, USA). An external pump was used for sampling at 5 SLM, and the flow rate was controlled by a MFC (Model CS200 Sevenstar Flow Co., Ltd., Beijing, China).

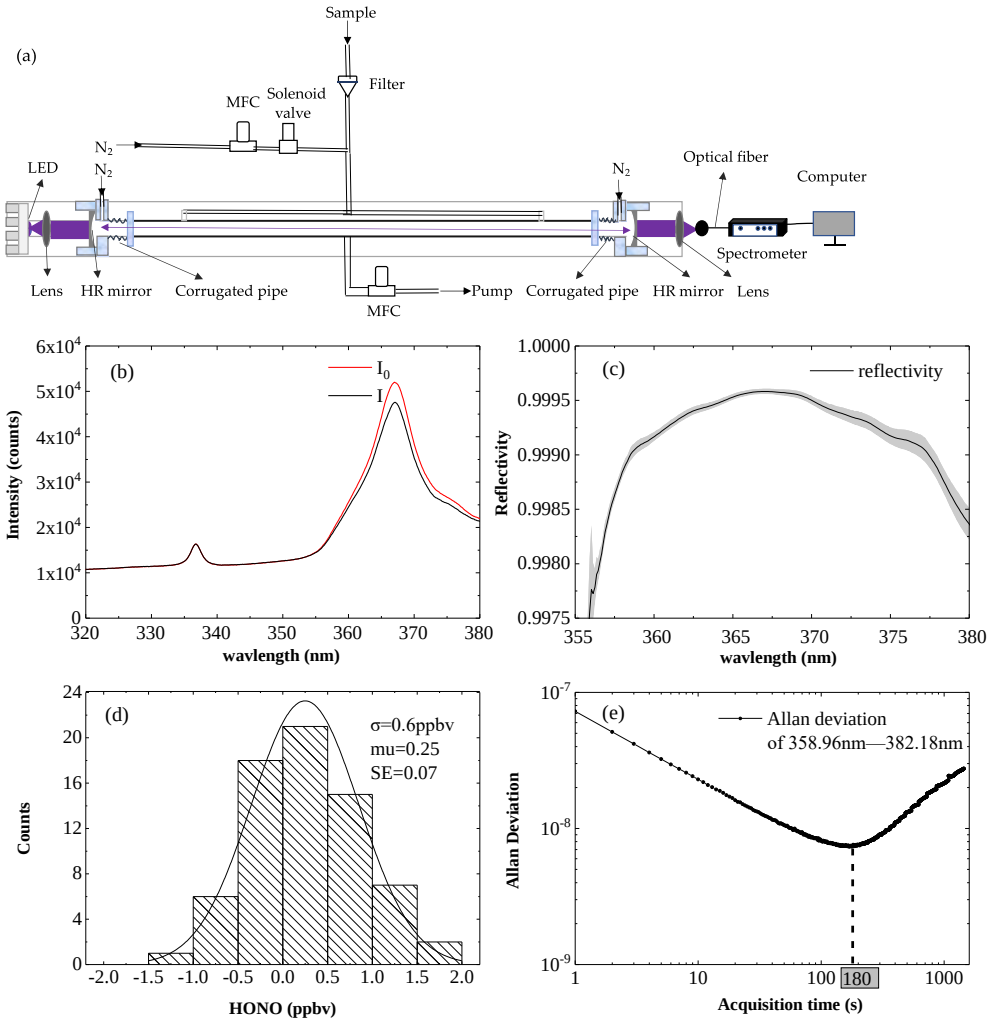


Figure 2. (**a**) Schematic of the IBBCEAS instrument. (**b**) The spectral intensity in the corresponding band measured by the spectrometer, I_0: spectrum with N_2 filling the cavity, I: spectrum with NO_2 filling the cavity. (**c**) Effective mirror reflectivity spectrum retrieved with errors. (**d**) HONO concentration distribution and Gaussian fit from experiments with calibration gases. (**e**) Allan variance plot for optimization of the data acquisition parameters.

Data processing: A program developed in LabVIEW was used for collecting spectra and processing of the same parameters such as HONO and NO_2 cross sections obtained from the literature [51,52], which were convolved into the spectrometer resolution, and the concentrations were retrieved using a linear least square analysis based on a singular value decomposition (SVD) method [53].

2.2.2. Reflectivity Calibration of IBBCEAS-HONO

It is important to ensure that an effective reflectivity of the mirrors constituting the cavity is calibrated. The signal was optimized and obtained as shown in Figure 2b. The peak at 336.76 nm was used to normalize I_0 based on a previous study [54]. There are two conventional methods for calibrating the high reflection mirror: (1) Use nitrogen as the zero gas to obtain the stable spectral signal I_0, and then switch to the gas with known concentration and obtain the spectral signal I, then the reflectivity is calculated from the measured absorption coefficient [55]. (2) Two gases with a known Rayleigh scattering cross section are introduced in a sequential manner, and the reflectivity is retrieved from the measured spectra and known cross sections [29]. The first method is selected for calibration in this work. First, N_2 with a high purity of 99.999% is introduced for at least 30 min to obtain a stable background spectrum I_0. Then, one can switch to the set concentration of

NO_2 gas into the cavity and obtain its absorption spectrum *I*. Considering the instability of NO_2 standard gas, an NO_x analyzer (Chemiluminescence detector, Thermofisher-42i) was connected in order to online determine the concentration of NO_2 gas. Considering the repeatability of calibration, four NO_2 gases with different concentrations were for calibration and corresponding error estimation. The effective reflectivity R of the high reflection mirror pair as calculated according to Equation (5) is shown in Figure 2c, with a maximum of > 0.9995 in the central spectral band.

$$R = 1 - \frac{n \cdot \sigma \cdot L_{IBBCEAS}}{\frac{I_0}{I} - 1} \tag{5}$$

2.2.3. Detection Limits of IBBCEAS-HONO

The standard variance and Allan's variance is used to characterize the detection limits and the stability of the instrument. This method determines the stability of the device by continuously measuring a blank sample (N_2 is used as the blank sample in this paper) and finally calculating the variance between two adjacent samples. In the Allan variance, the influence of the noise source on the system can be calculated for different integration times such that the stability corresponding to the actual integration time used can be evaluated. The calculation method is shown in Equation (6).

$$X_{p,i}(K) = \frac{1}{K}\Sigma_{m=1}^{K} Y_{p,(i-1)K+m}, i = 1, 2, 3 \ldots M, M = \frac{N}{K} \tag{6}$$

The continuous spectrum (*p* is the number of wavelength points in the band taken, *p* =1, 2, 3, 4 … … ; *i* = 1, 2, 3, 4 … … *N*) is divided into *M* groups, each containing *K* spectra, and the K spectra in each group are averaged. The Allan variance of these averages at each wavelength point can be calculated according to Equation (7).

$$\sigma_A^2(P, K) = \frac{1}{2(M-1)}\Sigma_{i=1}^{M-1}\left(X_{p,i+1}(K) - X_{p,i}(K)\right)^2 \tag{7}$$

The average Allan variance of all wavelength points is shown in Equation (8).

$$\sigma_A^2(K) = \frac{1}{P}\Sigma_{P=1}^{P}\sigma_A^2(P, K) \tag{8}$$

The detection limit of the system can be improved by increasing the integration time of the spectrometer (the spectrometer cannot be saturated) and the number of spectra. Theoretically, the signal-to-noise ratio is proportional to $\sqrt{t}$, where t is the integration time. In the real situation, the light intensity is affected due to the instability of the emission spectrum of the light source and the detector of the spectrometer. Hence, the integration time increased, and the enhancement of the signal-to-noise ratio was less than the estimated theoretical value. Systematic fluctuations can be removed by the fitting of the absorption spectra during the analysis for the determination of concentrations; thus, the source or detector instabilities (affecting as a jump in the measured intensity uniformly at all wavelengths) cannot truly reflect the instabilities in the measurement results. To calculate the Allan variance, the first measured N_2 spectrum was used as I_0 under different time resolution conditions, and each extinction spectrum was fit to the absorption cross section by the SVD routine to give a range of HONO concentrations. The results of the concentration distribution fitting are shown in Figure 2d below, its mean value is 0.25 ppbv, standard deviation σ = 0.6 ppbv, and mean standard error is 0.07 ppbv. The Allan variance for this time resolution condition gives a true indication of the stability of the system measurements. As shown in Figure 2e of the Allan variance, the optimum integration time for HONO is 180 s, and the detection limit is 0.76 ppbv, obtained from the standard variance.

2.2.4. Sampling Residence Time of IBBCEAS-HONO

IBBCEAS, as a detection method, is suitable for many scenarios: fixed-point atmospheric observation, vertical gradient distribution measurement, emission sources monitoring, mobile monitoring, etc. It is necessary to determine whether the sampling can be suitable for the application effectively. A suitable sampling flow rate ensures that the measured sample residence time is optimized. Experiments were carried out as follows in the laboratory to characterize the suitable sampling flow rate.

The saturated gaseous nitrophenol has strong absorption at near-UV [29]. It was injected into the sampling port of IBBCEAS setup by a micro-injector, and the sampling flow rate was controlled by an MFC (max. 20 SLM). The signal decreased when the sample was injected, and then it returned to the initial signal level. Afterward, the next sample injection can be performed. A total of 11 different flow rates were set, and each flow rate was repeated 5 times to ensure the repeatability of the results. The trend of central band signal (1 s time res.) showed the residence time when the sample passed through the cavity. The sampling flow rates corresponding to the residence time of the setup are shown in Table 1 below. Based on this result, the most suitable sampling flow can be selected under the specified resolution and integration time requirements.

Table 1. Sample gas residence time corresponding to sampling flow.

Test No.	Sampling Flow Rate (L/min)	Residence Time (s)
1	1.2	18.8
2	1.6	14.4
3	1.8	13.2
4	2.0	12.8
5	2.2	12.2
6	2.4	11.6
7	2.6	10.8
8	2.8	8.6
9	3.0	7.2
10	4.0	6.0
11	5.0	5.0

2.3. Intercomparison Measurements

In this work, laboratory experiments followed by field observations were used to verify the consistency of the responses of IBBCEAS and LOPAP to HONO measurement, comparing the relationship between them.

A schematic of the laboratory experiments performed is shown in Figure 3a. Under 28% relative humidity, the standard gas cylinder of NO_2 (2000 ppbv) is diluted by N_2 with a multi-gas calibrator (Thermofisher-146i) to 400 ppbv NO_2 and then passed into the parallel sampling inlet of IBBCEAS and LOPAP in parallel.

The schematic of the field deployment strategy using the instruments for HONO measurements is shown in Figure 3b. Ambient monitoring was carried out from 30 December 2017 to 2 January 2018 at Shanghai, People's Republic of China, during which a typical particulate matter pollution period was encountered. This observation campaign was performed at the SAES monitoring site, which is located in the urban Shanghai area surrounded by transportation and building facilities. During the field observations, both IBBCEAS and LOPAP instrumentation were placed at the same elevation in close proximity to each other and sampled from the same sampling line to ensure proper intercomparison.

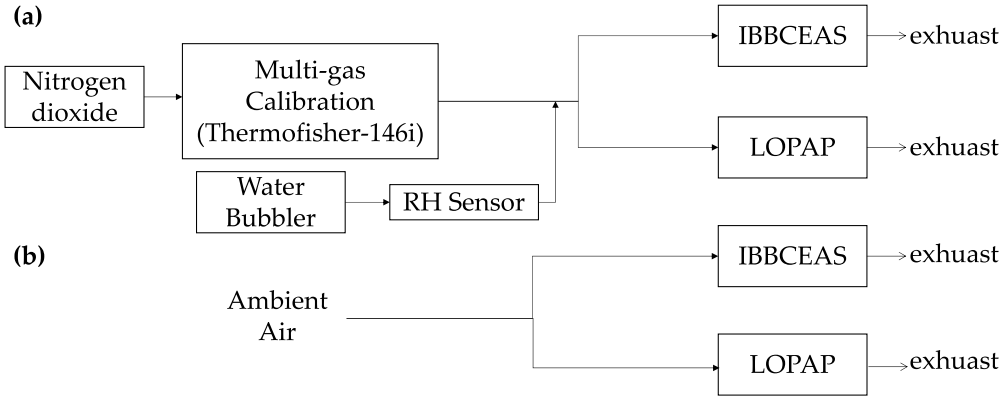


Figure 3. (**a**) Schematic diagram of parallel installation of IBBCEAS and LOPAP instrumentation in the laboratory. (**b**) Schematic diagram of parallel installation of IBBCEAS and LOPAP during the field observation.

3. Results and Discussion

3.1. Intercomparison of Laboratory Experiments

Prior to the start of the experiments, the IBBCEAS was calibrated for effective reflectivity to obtain an accurate concentration of target species. NO_2 from the gas-calibrator was introduced under 28% relative humidity. During the operation of LOPAP, the bubbles were often formed in the liquid phase, which makes the data unreliable at that time. Some unreliable data in the form of outliers were removed during the data analysis of LOPAP instrument. The time series of the NO_2 concentration and the HONO concentration is shown in Figure 4. It can be seen from Figure 4a that the NO_2 flow concentrations are diluted to about 150 ppbv by a multi-gas calibrator and measured by the IBBCEAS. Figure 4b shows laboratory-generated HONO measured by IBBCEAS (red trace) and LOPAP (bule trace). The measured concentrations from both instruments are shown to be in excellent agreement (see Figure 4).

It is clear that the two custom-developed instruments, both IBBCEAS and HONO, have shown similar responses to HONO generated in the laboratory. The average concentrations recorded by IBBCEAS (1.62 ppbv) and LOPAP (1.55 ppbv) showed excellent correlation. This excellent agreement in the results demonstrated the feasibility of IBBCEAS as an alternative method for HONO measurements. Furthermore, both instruments can be employed in field observations for intervalidating HONO concentrations, thus ensuring the accuracy of the retried concentrations.

3.2. Intercomparison of Ambient Air Measurements

During a winter field campaign at the end of 2017, IBBCEAS and LOPAP measured ambient HONO simultaneously. The measurement time resolutions were 1 and 5 min, respectively. Considering the reasonable validity of the laboratory data, both instruments were deployed for a continuous field observation for three consecutive days between 30 December 2017 and 2 January 2018. The atmospheric HONO concentrations measured by both instruments were interpolated to obtain the same time resolution.

Figure 5a shows that the HONO concentration measured by IBBCEAS (red trace) and LOPAP (blue trace) during the 3-day field deployment are in good agreement. In addition, both have obvious diurnal variation such that HONO accumulates during the night and begins to be photolyzed in the morning. Motor vehicular emissions and special circumstances will increase the concentration of HONO to form a daytime peak. These are in line with our understandings of the urban HONO sources [56].

The overall HONO concentrations ranged from 0–4 ppbv, with maximum HONO concentrations of 3.19 and 3.77 ppbv measured by IBBCEAS and LOPAP, respectively; the mean concentrations were 1.28 ppbv and 1.20 ppbv. It may be that the NO_2 pollution is severe during this period, which makes the concentration of heterogeneous formation of

NO_2 converted to HONO higher. At the same time, motor vehicular exhaust emissions, coal burning in winter, and other primary sources lead to high HONO concentrations, while in winter, the intensity of light radiation is lower, leading to a decrease in HONO photolysis efficiency. Therefore, the overall high HONO concentration as observed here was expected.

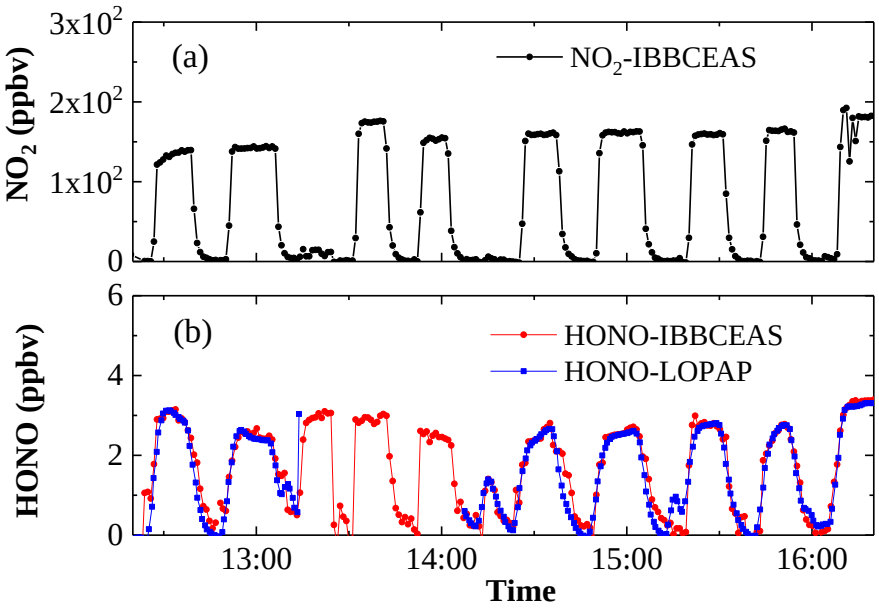


Figure 4. (**a**) Time series of NO_2 concentration under laboratory experimental conditions. (**b**) Time series of concentration of HONO-IBBCEAS and HONO-LOPAP averaged to the same time intervals.

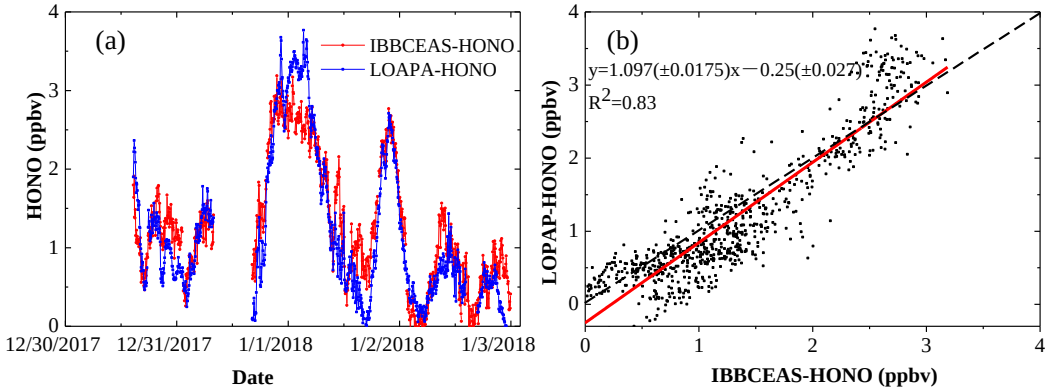


Figure 5. (**a**) The time series of HONO measured by IBBCEAS and LOPAP in Shanghai from 30 December 2017 to 2 January 2018. (**b**) Correlation plot of time series of HONO concentration measurements from the IBBCEAS instrument and the LOPAP over four days between 30 December 2017 and 2 January 2018. The red line is the correlation fit curve, and the black dashed line is y = x.

In Figure 5b, LOPAP and IBBCEAS data were compared, and correlation and regression analyses were performed as follows. The correlation of LOPAP-HONO vs. IBBCEAS-HONO has been obtained with R^2 = 0.83, a slope of 1.097 ± 0.0175, and an intercept of −0.25 ± 0.027. The intercept here is reasonable according to the detection limits of IBBCEAS and LOPAP, and the agreement demonstrates the IBBCEAS technique's feasibility for measuring ambient HONO. The discrepancy of 9.7% ± 1.75% in the observation can be attributed to the zero spectra I_0 and any errors in the mirror reflectivity R calibrations and drifts thereof. Frequent acquisition of reference spectra as well as reflectivity calibrations are suggested to avoid such drifts. In particular, the zero spectra I_0 play a significant role in

the concentration retrieval from the recorded spectra, which were also observed in previous studies [57]. An ideal measurement approach to eliminate the errors from light source intensity variation is to design an IBBCEAS setup in a dual-cavity configuration as reported by Chandran et al. in 2017 [58], where they simultaneously monitored the reference cavity transmission signal together with the sample cavity transmission signal.

4. Conclusions

In summary, from intercomparison of laboratory experiments and atmospheric observations, the IBBCEAS-HONO instrument and LOPAP-HONO instrument were calibrated and mutually verified with the accuracy of the data adequate for ambient measurements in a polluted urban atmosphere. During the measurement of atmospheric HONO, some discrepancies between the instruments were observed, which indicate that the measurement of HONO is still challenging, and the IBBCEAS must have frequent calibration and reference spectral acquisition to avoid drifts.

Author Contributions: Methodology, Formal analysis, Writing—original draft preparation, Z.Y.; Methodology, Data curation, M.W., Y.H. and Y.L.; Software, Data curation, S.C. and R.V.; Validation, Project administration, S.L.; Conceptualization, Writing—review and editing, Supervision, Funding acquisition, J.C.; All authors have read and agreed to the published version of the manuscript.

Funding: This research was funded by National Natural Science Foundation of China (grant nos. 91544225), the National Key Research and Development Program of China (grant nos. 2018YFC0213800 and 2017YFC0211500, respectively).

Conflicts of Interest: The authors declare no conflict of interest.

References

1. Elshorbany, Y.F.; Kleffmann, J.; Kurtenbach, R.; Lissi, E.; Rubio, M.; Villena, G.; Gramsch, E.; Rickard, A.R.; Pilling, M.J.; Wiesen, P. Seasonal dependence of the oxidation capacity of the city of Santiago de Chile. *Atmos. Environ.* **2010**, *44*, 5383–5394. [CrossRef]
2. Elshorbany, Y.F.; Kleffmann, J.; Hofzumahaus, A.; Kurtenbach, R.; Wiesen, P.; Dorn, H.P.; Schlosser, E.; Brauers, T.; Fuchs, H.; Rohrer, F.; et al. HO_x budgets during HO_xComp: A case study of HO_x chemistry under NO_x limited conditions. *J. Geophys. Res.* **2012**, *117*, 812–819. [CrossRef]
3. Alicke, B.; Platt, U.; Stutz, J. Impact of nitrous acid photolysis on the total hydroxyl radical budget during the Limitation of Oxidant Production/Pianura Padana Produzione di Ozono study in Milan. *J. Geophys. Res.* **2002**, *107*, 8196. [CrossRef]
4. Alicke, B. OH formation by HONO photolysis during the BERLIOZ experiment. *J. Geophys. Res.* **2003**, *108*, 8247–8263. [CrossRef]
5. Vogel, B.; Vogel, H.; Kleffmann, J.; Kurtenbach, R. Measured and simulated vertical profiles of nitrous acid—Part II. Model simulations and indications for a photolytic source. *Atmos. Environ.* **2003**, *37*, 2957–2966. [CrossRef]
6. Kleffmann, J.; Kurtenbach, R.; Lorzer, J.; Wiesen, P.; Kalthoff, N.; Vogel, B.; Vogel, H. Measured and simulated vertical profiles of nitrous acid—Part I: Field measurements. *Atmos. Environ.* **2003**, *37*, 2949–2955. [CrossRef]
7. Kleffmann, J.; Gavriloaiei, T.; Hofzumahaus, A.; Holland, F.; Koppmann, R.; Rupp, L.; Schlosser, E.; Siese, M.; Wahner, A. Daytime formation of nitrous acid: A major source of OH radicals in a forest. *Geophys. Res. Lett.* **2005**, *32*, 347–354. [CrossRef]
8. Ren, X.R.; Harder, H.; Martinez, M.; Lesher, R.L.; Oliger, A.; Simpas, J.B.; Brune, W.H.; Schwab, J.J.; Demerjian, K.L.; He, Y.; et al. OH and HO_2 chemistry in the urban atmosphere of New York City. *Atmos. Environ.* **2003**, *37*, 3639–3651. [CrossRef]
9. Finlayson-Pitts, B.J.; Pitts, J.N., Jr. *Chemistry of the Lower and Upper Atmosphere: Theory, Experiments and Applications*; Academic Press: New York, NY, USA, 2000.
10. Harrison, R.M.; Peak, J.D.; Collins, G.M. Tropospheric cycle of nitrous acid. *J. Geophys. Res.* **1996**, *101*, 14429–14439. [CrossRef]
11. Nash, T. Nitrous acid in the atmosphere and laboratory experiments on its photolysis. *Tellus* **1974**, *26*, 175–179. [CrossRef]
12. Perner, D.; Platt, U. Detection of nitrous acid in the atmosphere by differential optical absorption. *Geophys. Res. Lett.* **1979**, *6*, 917–920. [CrossRef]
13. Stutz, J.; Wong, K.W.; Tsai, C. Field Observation of Daytime HONO Chemistry and its Impact on the OH Radical Budget. In *Disposal of Dangerous Chemicals in Urban Areas and Mega Cities*; Barnes, I., Rudzinski, K.J., Eds.; NATO Science for Peace and Security Series C: Environmental Security; Springer: Dordrecht, The Netherlands, 2013.
14. Kurtenbach, R.; Becker, K.H.; Gomes, J.A.G.; Kleffmann, J.; Lörzer, J.C.; Spittler, M.; Wiesen, P.; Ackermann, R.; Geyer, A.; Platt, U.; et al. Investigations of emissions and heterogeneous formation of HONO in a road traffic tunnel. *Atmos. Environ.* **2001**, *35*, 3385–3394. [CrossRef]
15. Qin, M.; Liu, W.; Xie, P.; Liu, J.; Fang, W.; Zhang, W. Study progress on the source of atmospheric HONO. *Environ. Monit. China* **2005**, *21*, 82–88.
16. Su, H.; Cheng, Y.; Oswald, R.; Behrendt, T.; Trebs, I.; Meixner, F.X.; Andreae, M.O.; Cheng, P.; Zhang, Y.; Pöschl, U. Soil nitrite as a source of atmospheric HONO and OH radicals. *Science* **2011**, *333*, 1616–1618. [CrossRef] [PubMed]

17. Li, X.; Brauers, T.; Häseler, R.; Bohn, B.; Fuchs, H.; Hofzumahaus, A.; Holland, F.; Lou, S.; Lu, K.D.; Rohrer, F.; et al. Exploring the atmospheric chemistry of nitrous acid (HONO) at a rural site in Southern China. *Atmos. Chem. Phys.* **2012**, *12*, 1497–1513. [CrossRef]
18. Finlayson-Pitts, B.J.; Wingen, L.M.; Sumner, A.L.; Syomin, D.; Ramazan, K.A. The heterogeneous hydrolysis of NO_2 in laboratory systems and in outdoor and indoor atmospheres: An integrated mechanism. *Phys. Chem. Chem. Phys.* **2003**, *5*, 223–242. [CrossRef]
19. Ndour, M.; D'Anna, B.; George, C.; Ka, O.; Balkanski, Y.; Kleffmann, J.; Stemmler, K.; Ammann, M. Photoenhanced uptake of NO_2 on mineral dust: Laboratory experiments and model simulations. *Geophys. Res. Lett.* **2008**, *35*, L05812. [CrossRef]
20. An, J.L.; Li, Y.; Tang, Y.J.; Chen, Y.; Qu, Y. Advances in HONO sources, HONO simulations, and the impacts of the HONO sources on regional or global air quality. *J. Environ. Sci.* **2014**, *34*, 273–281.
21. Zhou, X.L.; He, Y.; Huang, G.; Thornberry, T.D.; Carroll, M.A.; Bertman, S.B. Photochemical production of nitrous acid on glass sample manifold surface. *Geophys. Res. Lett.* **2002**, *29*, 1681. [CrossRef]
22. Bejan, I.; Abd-el-Aal, Y.; Barnes, I.; Benter, T.; Bohn, B.; Wiesen, P.; Kleffmann, J. The photolysis of ortho-nitrophenols: A new gas phase source of HONO. *Phys. Chem. Chem. Phys.* **2006**, *8*, 2028–2035. [CrossRef]
23. Spataro, F.; Ianniello, A. Sources of atmospheric nitrous acid: State of the science, current research needs, and future prospects. *J. Air Waste Manag.* **2014**, *64*, 1232–1250. [CrossRef] [PubMed]
24. Harrison, R.M.; Kitto, A.M.N. Evidence for a surface source of atmospheric nitrous acid. *Atmos. Environ.* **1994**, *28*, 1089–1094. [CrossRef]
25. Stutz, J.; Oh, H.J.; Whitlow, S.I.; Anderson, C.; Dibb, J.E.; Flynn, J.H.; Rappenglück, B.; Lefer, B. Simultaneous DOAS and mist-chamber IC measurements of HONO in Houston, TX. *Atmos. Environ.* **2010**, *44*, 4090–4098. [CrossRef]
26. Wang, L.; Zhang, J. Detection of Nitrous Acid by Cavity Ring-Down Spectroscopy. *Environ. Sci. Technol.* **2000**, *34*, 4221–4227. [CrossRef]
27. Schiller, C.L.; Locquiao, S.; Johnson, T.J.; Harris, G.W. Atmospheric Measurements of HONO by Tunable Diode Laser Absorption Spectroscopy. *J. Atmos. Chem.* **2001**, *40*, 275–293. [CrossRef]
28. Gherman, T.; Venables, D.S.; Vaughan, S.; Orphal, J.; Ruth, A.A. Incoherent broadband cavity-enhanced absorption spectroscopy in the near-ultraviolet: Application to HONO and NO_2. *Environ. Sci. Technol.* **2008**, *42*, 890–895. [CrossRef]
29. Chen, J.; Wenger, J.C.; Venables, D.S. Near-ultraviolet absorption cross sections of nitrophenols and their potential influence on tropospheric oxidation capacity. *J. Phys. Chem. A* **2011**, *115*, 12235–12242. [CrossRef]
30. Appel, B.R.; Winer, A.M.; Tokiwa, Y.; Biermann, H.W. Comparison of atmospheric nitrous acid measurements by annular denuder and differential optical absorption systems. *Atmos. Environ.* **1990**, *24*, 611–616. [CrossRef]
31. Heland, J.; Kleffmann, J.; Kurtenbach, R.; Wiesen, P. A new instrument to measure gaseous nitrous acid (HONO) in the atmosphere. *Environ. Sci. Technol.* **2001**, *35*, 3207–3212. [CrossRef]
32. Chen, L.; Hou, S.Q.; Wang, W.G.; Tong, S.R.; Pei, K.M.; Ge, M.F. Development of a home-made long path absorption photometer for the sensitive detection of nitrous acid. *Acta Phys. Sin.* **2014**, *30*, 1408–1415.
33. Reisinger, A.R. Observations of HNO_2 in the polluted winter atmosphere: Possible heterogeneous production on aerosols. *Atmos. Environ.* **2000**, *34*, 3865–3874. [CrossRef]
34. Kleffmann, J.; Wiesen, P. Technical Note: Quantification of interferences of wet chemical HONO LOPAP measurements under simulated polar conditions. *Atmos. Chem. Phys.* **2008**, *8*, 6813–6822. [CrossRef]
35. Kleffmann, J. Daytime sources of nitrous acid (HONO) in the atmospheric boundary layer. *Chem. Phys. Chem.* **2007**, *8*, 1137–1144. [CrossRef] [PubMed]
36. Xue, C.; Ye, C.; Ma, Z.; Liu, P.; Zhang, Y.; Zhang, C.; Tang, K.; Zhang, W.; Zhao, X. Development of stripping coil-ion chromatograph method and intercomparison with CEAS and LOPAP to measure atmospheric HONO. *Sci. Total Environ.* **2019**, *646*, 187–195. [CrossRef]
37. Dixneuf, S.; Ruth, A.; Häseler, R.; Brauers, T.; Rohrer, F.; Dorn, H.P. Comparison of nitrous acid detection using open-path incoherent broadband cavity-enhanced absorption spectroscopy and extractive long-path absorption photometry. *Atmos. Meas. Tech.* **2021**, *291*, 1–28.
38. Yi, H.; Cazaunau, M.; Gratien, A.; Michoud, V.; Pangui, E.; Doussin, J.F.; Chen, W. Intercomparison of IBBCEAS, NitroMAC and FTIR analyses for HONO, NO_2 and CH_2O measurements during the reaction of NO_2 with H_2O vapour in the simulation chamber CESAM. *Atmos. Meas. Tech.* **2021**, *14*, 5701–5715. [CrossRef]
39. Saltzman, B.E. Colorimetric Micro-determination of Nitrogen Dioxide in Atmosphere. *Anal. Chem.* **1954**, *26*, 1949–1955. [CrossRef]
40. Kleffmann, J.; Lörzer, J.C.; Wiesen, P.; Kern, C.; Trick, S.; Volkamer, R.; Ródenas, M.; Wirtz, K. Intercomparison of the DOAS and LOPAP techniques for the detection of nitrous acid (HONO). *Atmos. Environ.* **2006**, *40*, 3640–3652. [CrossRef]
41. Häseler, R.; Brauers, T.; Holland, F.; Wahner, A. Development and application of a new mobile LOPAP instrument for the measurement of HONO altitude profiles in the planetary boundary layer. *Atmos. Meas. Tech. Discuss.* **2009**, *2*, 2027–2054.
42. Liu, Y.; Lu, K.; Dong, H.; Li, X.; Cheng, P.; Zou, Q.; Wu, Y.; Liu, X.; Zhang, Y. In situ monitoring of atmospheric nitrous acid based on multi-pumping flow system and liquid waveguide capillary cell. *J. Environ. Sci.* **2016**, *43*, 273–284. [CrossRef]
43. Villena, G.; Bejan, I.; Kurtenbach, R.; Wiesen, P.; Kleffmann, J. Development of a new Long Path Absorption Photometer (LOPAP) instrument for the sensitive detection of NO_2 in the atmosphere. *Atmos. Meas. Tech.* **2011**, *4*, 1663–1676. [CrossRef]
44. Peters, S.; Bejan, I.; Kurtenbach, R.; Liedtke, S.; Villena, G.; Wiesen, P.; Kleffmann, J. Development of a new LOPAP instrument for the detection of O_3 in the atmosphere. *Atmos. Environ.* **2013**, *67*, 112–119. [CrossRef]

45. Wu, T.; Zha, Q.; Chen, W.; Xu, Z.; Wang, T.; He, X. Development and deployment of a cavity enhanced UV-LED spectrometer for measurements of atmospheric HONO and NO_2 in Hong Kong. *Atmos. Environ.* **2014**, *95*, 544–551. [CrossRef]
46. Donaldson, M.A.; Berke, A.E.; Raff, J.D. Uptake of Gas Phase Nitrous Acid onto Boundary Layer Soil Surfaces. *Environ. Sci. Technol.* **2014**, *48*, 375–383. [CrossRef]
47. Scharko, N.K.; Berke, A.E.; Raff, J.D. Release of Nitrous Acid and Nitrogen Dioxide from Nitrate Photolysis in Acidic Aqueous Solutions. *Environ. Sci. Technol.* **2014**, *48*, 11991–12001. [CrossRef] [PubMed]
48. Min, K.E.; Washenfelder, R.A.; Dubé, W.P.; Langford, A.O.; Edwards, P.M.; Zarzana, K.J.; Stutz, J.; Lu, K.; Rohrer, F.; Zhang, Y. A broadband cavity enhanced absorption spectrometer for aircraft measurements of glyoxal, methylglyoxal, nitrous acid, nitrogen dioxide, and water vapor. *Atmos. Meas. Tech.* **2016**, *9*, 423–440. [CrossRef]
49. Nakashima, Y.; Sadanaga, Y. Validation of in situ Measurements of Atmospheric Nitrous Acid Using Incoherent Broadband Cavity-enhanced Absorption Spectroscopy. *Anal. Sci.* **2017**, *33*, 519–524. [CrossRef]
50. Duan, J.; Qin, M.; Ouyang, B.; Fang, W.; Li, X.; Lu, K.; Tang, K.; Liang, S.; Meng, F.; Hu, Z.; et al. Development of an incoherent broadband cavity enhanced absorption spectrometer for in situ measurements of HONO and NO_2. *Atmos. Meas. Tech.* **2018**, *11*, 4531–4543. [CrossRef]
51. Stutz, J.; Kim, E.S.; Platt, U.; Bruno, P.; Perrino, C.; Febo, A. UV-visible absorption cross sections of nitrous acid. *Geophys. Res.* **2000**, *105*, 14585–14592. [CrossRef]
52. Voigt, S.; Orphal, J.; Burrows, J.P. The temperature and pressure dependence of the absorption cross-sections of NO_2 in the 250-800 nm region measured by Fourier-transform spectroscopy. *Photochem. Photobiol. A Chem.* **2002**, *149*, 1–7. [CrossRef]
53. Suhail, K.; George, M.; Orphal, J.; Chandran, S.; Varma, R.; Venables, D.S.; Wang, M.; Chen, J. Open path incoherent broadband cavity-enhanced measurements of NO_3 radical and aerosol extinction in the North China Plain. *Spectrochim. Acta Part A Mol. Biomol. Spectrosc.* **2019**, *208*, 24–31. [CrossRef] [PubMed]
54. Chen, J.; Fullam, D.P.; Yu, S.; Böge, O.; Le, P.H.; Herrmann, H.; Venables, D.S. Improving the accuracy and precision of broadband optical cavity measurements. *Spectrochim. Acta Part A Mol. Biomol. Spectrosc.* **2019**, *218*, 178–183. [CrossRef] [PubMed]
55. Venables, D.S.; Gherman, T.; Orphal, J.; Wenger, J.C.; Ruth, A.A. High sensitivity in situ monitoring of NO3 in an atmospheric simulation chamber using incoherent broadband cavity-enhanced absorption spectroscopy. *Environ. Sci. Technol.* **2006**, *40*, 6758. [CrossRef] [PubMed]
56. Pinto, J.P.; Dibb, J.; Lee, B.H.; Rappengluck, B.; Wood, E.C.; Levy, M.; Zhang, R.; Lefer, B.; Ren, X.; Stutz, J.; et al. Intercomparison of field measurements of Nitrous Acid (HONO) during the SHARP campaign. *J. Geophys. Res-Atmos.* **2014**, *119*, 5583–5601. [CrossRef]
57. Fuchs, H.; Ball, S.M.; Bohn, B.; Brauers, T.; Cohen, R.C.; Dorn, H.P.; Dubé, W.P.; Fry, J.L.; Häseler, R.; Heitmann, U. Intercomparison of measurements of NO_2 concentrations in the atmosphere simulation chamber SAPHIR during the NO_3 Comp campaign. *Atmos. Meas. Tech.* **2010**, *3*, 21–37. [CrossRef]
58. Chandran, S.; Puthukkudy, A.; Varma, R. Dual-wavelength dual-cavity spectrometer for NO_2 detection in the presence of aerosol interference. *Appl. Phys. B* **2017**, *123*, 1–8. [CrossRef]